Bis(triarylmethylium)-type Macrocyclic Dications: Mechanochromic Emission Extending to the Red Region

Yusuke Ishigaki,*[a] Takuya Tachibana,[a] Kazuma Sugawara,[a] Moto Kikuchi,[a] and Takanori Suzuki[a]

[a] Prof. Dr. Y. Ishigaki, T. Tachibana, Dr. K. Sugawara, M. Kikuchi, Prof. Dr. T. Suzuki
Department of Chemistry, Faculty of Science
Hokkaido University
Sapporo, Hokkaido 060-0810 (Japan)
E-mail: yishigaki@sci.hokudai.ac.jp

Supporting information for this article is given via a link at the end of the document.

Abstract: Macrocyclic dications $\mathbf{2}^{2+}$ composed of two triarylmethylium units were designed and synthesized. In contrast to the reference monocations $\mathbf{1}^{+}$, macrocyclic dications $\mathbf{2}^{2+}$ exhibited mechanochromic emission extending to the red region (~900 nm), since the luminescence color in a solid state can reversibly change due to their constrained structures granted by alkylene linkers and the choice of a proper counterion. X-ray diffraction and spectroscopic analyses revealed that such mechanochromic behavior was induced by the crystal-to-amorphous transition. A change in the intermolecular interaction of macrocyclic dications $\mathbf{2}^{2+}$ would be the key to realizing a change in the emission pattern, since the color of the molecules did not change by applying mechanical stimuli. These findings may suggest a design strategy for creating a variety of stimuli-responsive materials, especially for carbocation-based fluorescent materials.

Introduction

Carbocations are widely known as intermediates in many chemical reactions and are generally unstable due to their high reactivity.[1] To attain chemical stability, resonance stabilization is of great importance for making carbocations stable, as seen in conjugated compounds, such as allyl and benzyl cations. In fact, triarylmethyliums are well-known as stable carbocations, and are potential candidates for applications as organic dyes because they have strong absorptions in the visible region due to the effective delocalization of π-electrons.[2] Since triarylmethyliums absorb visible light, their emissions can be extended to longer wavelengths than their absorptions. However, each aryl group in triarylmethyliums can freely rotate, so that rotatable triarylmethyliums do not have emissive properties in solution because of the fast non-radiative deactivation process (Figure 1).

By suppressing the free rotation of aryl groups, cationic helicenes and triangulenes, in which carbon, nitrogen, and/or oxygen atoms bridge two or three aryl groups at *ortho*-positions, show strong luminescence in solution (Figure 1).[3–6] Along these lines, a few studies have reported that triphenylmethyliums exhibit aggregation-induced emission (AIE)[7,8] on a film or silica surface, due to the suppressed rotation of phenyl groups. Furthermore, a propeller-like structure in an aggregated state reduces intermolecular interactions that cause emission quenching.

Such luminescent materials in an aggregated state have been actively studied due to their potential use for a wide range of applications such as bioimaging, displays, and devices.[9–11] In addition, molecules that reversibly change their color and/or luminescent behavior in response to mechanical stimuli such as grinding have attracted much attention in recent years due to their potential applications.[12–14] For example, mechanochromic molecules are expected to be used for mechanical sensors, the detection of defects and deformations, and secure printing, where luminescence in the long-wavelength region with deep penetration is required. However, there are only a few examples of mechanochromic organic molecules that exhibit luminescence in the red to near-infrared (NIR) region.[15–18]

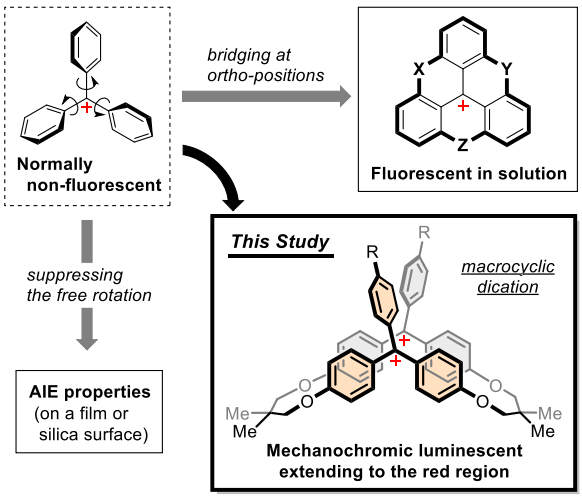

Figure 1. Design concept for this study.

Considering the response to mechanical stimulation in a solid state, flexible molecules or crystal packing would be important,[19] because they could adopt several conformations in different states (e.g., crystalline phase, amorphous) and their interconversion under the influence of external stimuli (e.g., grinding, heating, dissolving-drying) should give different emission properties.[14,20–26] Thus, we designed bis(triarylmethylium)-type macrocyclic dications $\mathbf{2}^{2+}$ with the expectation that they would exhibit a change in an intermolecular interaction in a solid state due to their constrained structures granted by alkylene linkers (Figure 1) and the reversibility could be modified by the choice of a proper counterion. By considering that carbocations such as triphenylmethyliums[27,28] and tropyliums[29] can exhibit emission

in the crystalline-state, we envisaged that macrocyclic dications would be promising candidates for solid-state luminescent materials, especially for NIR-emissive mechanochromic carbocations. In this study, we found that macrocyclic dications $\mathbf{2}^{2+}$ show red-emissive mechanochromic behavior based on a crystal-to-amorphous transition, while corresponding simple triarylmethyliums $\mathbf{1}^{+}$ do not exhibit such behavior due to the non-changeable molecular structure.

Results and Discussion

As shown in Scheme 1, cyclic diketone **6** was prepared by the reaction of 4,4'-dihydroxybenzophenone **3** with tosylated 2,2-dimethyl-1,3-propanediol **4**[30] in a stepwise manner. For the latter cyclic reaction, we adopted high dilution conditions (5 mM in DMF) and chose a *gem*-dimethyl substituted linker[31] with the expectation of efficient formation of an intramolecular cyclic compound rather than linear oligomers, and the desired compound **6**, the X-ray structure of which is shown in Figure S1, was isolated in 33% yield. When diketone **6** was reacted with the corresponding aryl lithium reagents, precursors **7'-F** and **7'-O** for dications were obtained in 81% and 92% yields, respectively, via intermediate diols **7-F** and **7-O**, which easily converted into dimethyl ether under reprecipitation conditions with MeOH. When **7'-F** and **7'-O** were subjected to acidic conditions, the target macrocyclic dication salts $\mathbf{2\text{-}F}^{2+}(BF_4^-)_2$ and $\mathbf{2\text{-}O}^{2+}(BF_4^-)_2$ were successfully isolated as red powders and stable entities. Single crystals of these dications were grown by a vapor diffusion method from CH_2Cl_2 solution under a hexane atmosphere, however, no suitable crystal of $\mathbf{2\text{-}O}^{2+}(BF_4^-)_2$ was obtained due to the low crystallinity. Thus, dication $\mathbf{2\text{-}O}^{2+}$ with different counter anions $(PF_6^-)_2$ was prepared in a similar manner.

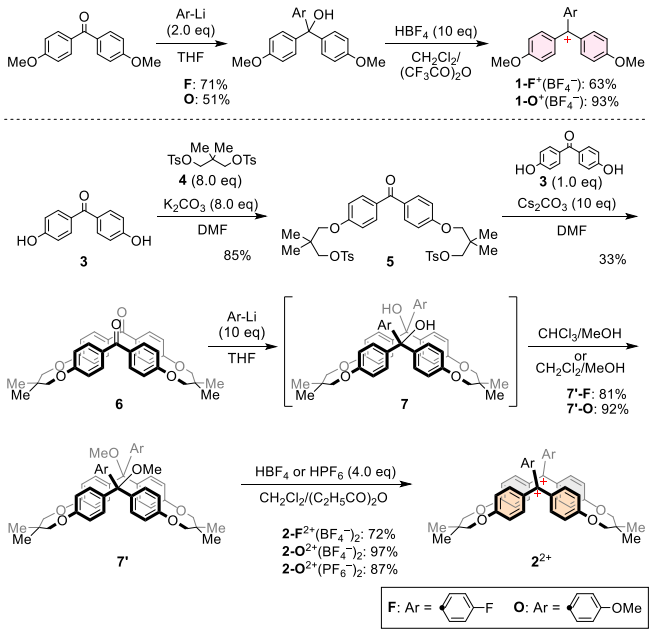

Scheme 1. Synthesis of monocations $\mathbf{1\text{-}F}^{+}(BF_4^-)$ and $\mathbf{1\text{-}O}^{+}(BF_4^-)$ and macrocyclic dications $\mathbf{2\text{-}F}^{2+}(BF_4^-)_2$, $\mathbf{2\text{-}O}^{2+}(BF_4^-)_2$, and $\mathbf{2\text{-}O}^{2+}(PF_6^-)_2$.

Then, we conducted single-crystal X-ray analyses. For the crystal of monocation salt $\mathbf{1\text{-}F}^{+}(BF_4^-)$, each molecule is slip-stacked with the shortest intermolecular C···C contact of 3.332(2) Å (Figure S2), which is smaller than the sum of the van der Waals (vdW) radii (3.4 Å).[32] For the crystal of macrocyclic dication salt $\mathbf{2\text{-}F}^{2+}(BF_4^-)_2$, two chromophores in the molecule are facing each other and parallelly stacked (Figure 2a). As shown in Figure 2b, a quite similar molecular structure was determined by X-ray analysis of methoxyphenyl analogue $\mathbf{2\text{-}O}^{2+}(PF_6^-)_2$. Such compact structure is suitable for a change in an intermolecular interaction in a solid state by applying the mechanical force.

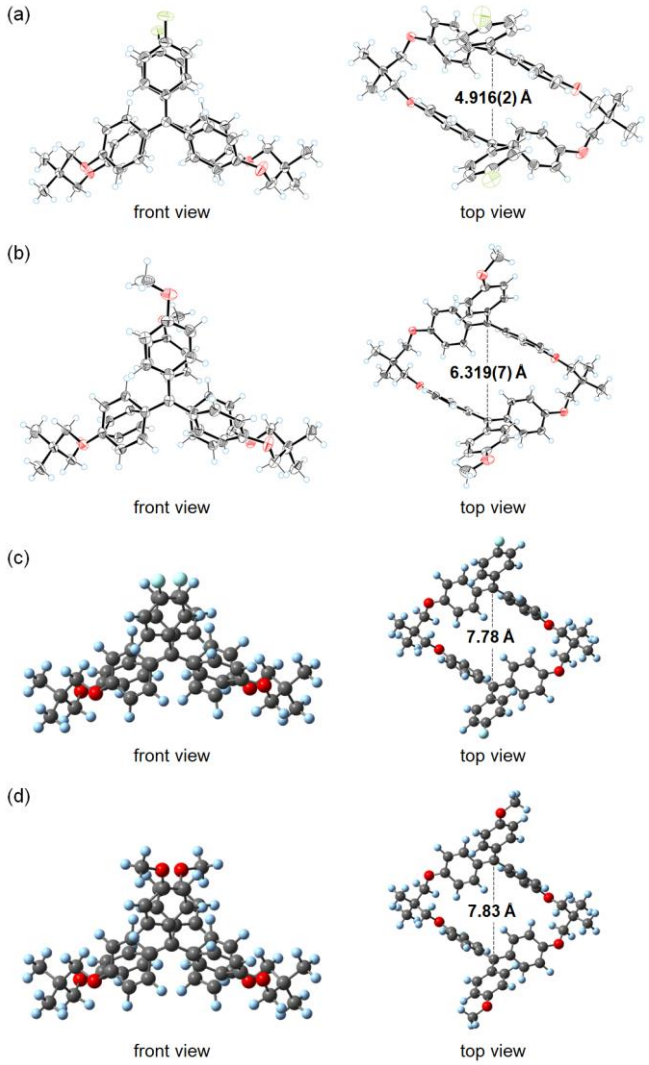

Figure 2. X-ray structures (ORTEP drawings) of (a) $\mathbf{2\text{-}F}^{2+}(BF_4^-)_2{\cdot}0.5(CH_2Cl_2)$ and (b) $\mathbf{2\text{-}O}^{2+}(PF_6^-)_2{\cdot}2(CH_2Cl_2)$. Thermal ellipsoids are shown at the 50% probability level. Counterions and solvent molecules are omitted for clarity. Optimized structures (with no imaginary frequency) of (a) $\mathbf{2\text{-}F}^{2+}$ and (b) $\mathbf{2\text{-}O}^{2+}$ based on DFT calculations (B3LYP/6-31G*).

To gain further insight into the molecular structure and molecular orbitals, we conducted density functional theory (DFT) calculations at the B3LYP-6-31G* level. The structure and frontier orbitals of macrocyclic dications $\mathbf{2}^{2+}$ are quite different between calculations using optimized and observed geometries. For example, the distances between the cation-centered carbon atoms in the optimized structure [7.78 Å for $\mathbf{2\text{-}F}^{2+}$ and 7.83 Å for $\mathbf{2\text{-}O}^{2+}$] are greater than those in the crystal [4.916(2) Å for $\mathbf{2\text{-}F}^{2+}(BF_4^-)_2$ and 6.319(7) Å for $\mathbf{2\text{-}O}^{2+}(PF_6^-)_2$] (Figure 2). The

intramolecular two triarylmethyliums are likely forced to be packed closely in the crystal. When we focus on the molecular orbitals of $\mathbf{2}^{2+}$ with the geometries obtained by X-ray analyses and DFT calculations (B3LYP-6-31G*), there is a significant difference. Compared to the DFT results with the optimized structure, the C_2-symmetry of the molecule is broken with the crystallographic coordinates, and thus the degeneracy of HOMO and LUMO is lifted (Figure S6). In this way, we considered that the photophysical properties would be different in a solid state with nondegenerate molecular orbitals and in solution, where the molecule could have degenerate molecular orbitals as in the gas phase.

First, we performed UV/Vis measurement in CH_2Cl_2. As shown in Figure 3, these macrocyclic dications exhibit strong absorptions in the visible region [λ_{max}/nm (log ε): 515 (sh, 4.45), 480 (5.09), 420 (4.78) for **2-F**$^{2+}$(BF_4^-)$_2$ and 476 (5.14), 455 (sh, 5.07) for **2-O**$^{2+}$(BF_4^-)$_2$, respectively]. Compared to reference monocations[33,34] [λ_{max}/nm (log ε): 503 (4.87), 421 (4.53) for **1-F**$^+$(BF_4^-) and 486 (5.03), 455 (sh, 4.67) for **1-O**$^+$(BF_4^-), respectively], which were prepared as shown in Scheme 1, obvious blue-shift of the first absorption band was observed for $\mathbf{2}^{2+}$. Since such blue-shift is a characteristic feature of H-aggregates,[35,36] two chromophore in the molecule are facing each other and parallelly stacked in solution. Furthermore, as a result of the intramolecular H-aggregates, the molar absorption coefficients of macrocyclic dications $\mathbf{2}^{2+}$ were less than twice those of monocations $\mathbf{1}^+$. The differences between fluorophenyl-substituted cations **1-F**$^+$ and **2-F**$^{2+}$ are greater than those between methoxyphenyl-substituted cations **1-O**$^+$ and **2-O**$^{2+}$, probably because the less stable dication **2-F**$^{2+}$ with fluorophenyl groups would need to gain further stabilization to adopt more closely packed structure, which is in accord with the fact that the distances between the cation-centered carbon atoms in fluorophenyl derivatives are shorter than those in methoxyphenyl derivatives.

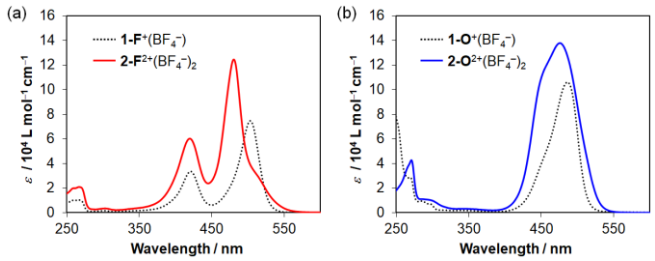

Figure 3. UV/Vis spectra of (a) **1-F**$^+$(BF_4^-) and **2-F**$^{2+}$(BF_4^-)$_2$, and (b) **1-O**$^+$(BF_4^-) and **2-O**$^{2+}$(BF_4^-)$_2$ in CH_2Cl_2.

To elucidate the detailed photophysical properties of monocations $\mathbf{1}^+$ and macrocyclic dications $\mathbf{2}^{2+}$, we conducted DFT calculations. As shown in Figures S3 and S4, HOMOs and LUMOs are highly delocalized on aryl groups for all cations with an optimized geometry based on calculations at the B3LYP/6-31G* level. The energy gap between HOMO and LUMO was estimated to be 3.00 eV and 3.08 eV for **1-F**$^+$ and **1-O**$^+$, respectively. Thus, the absorption bands in the visible region were assigned to a HOMO-LUMO transition, which was also supported by time-dependent (TD)-DFT calculations (Figure S5). For dications $\mathbf{2}^{2+}$, degenerated HOMOs and LUMOs were predicted to be located on both triarylmethylium units based on DFT calculations (B3LYP/6-31G*) by using optimized structures. As a result of degeneration of HOMOs and LUMOs, blue-shift and splitting of the absorptions can be observed in the UV/Vis spectra of $\mathbf{2}^{2+}$. TD-DFT calculations revealed that the absorptions around 400-500 nm correspond to several transitions, e.g., HOMO–1-LUMO, HOMO–1-LUMO+1, and HOMO–3-LUMO (Table S2). Based on the presence of electronic interaction between triarylmethyliums, macrocyclic dications $\mathbf{2}^{2+}$ exhibit unique absorption properties.

Since none of the carbocations have emissive properties in solution, as expected, we turned our attention to their solid-state properties. Solid-state samples of carbocations $\mathbf{1}^+$ and $\mathbf{2}^{2+}$ exhibit emission in longer-wavelength regions under UV light (Table 1). Orange and red emission were observed for as-synthesized powders of fluorophenyl-substituted cations [λ_{em}/nm (Φ_{em}): 609, 669 (0.03) for **1-F**$^+$(BF_4^-) and 642 (0.03) for **2-F**$^{2+}$(BF_4^-)$_2$], respectively. When crystalline powders of non-tethered monocation **1-F**$^+$(BF_4^-) were ground with an agate mortar and pestle, the emission at 669 nm and the quantum yield slightly decreased (Figure S8 and Table 1). However, almost the same patterns assigned to a crystalline phase were observed by powder X-ray diffraction (PXRD) before and after grinding, and thus the observed change of **1-F**$^+$(BF_4^-) is not considered as mechanochromic behavior.

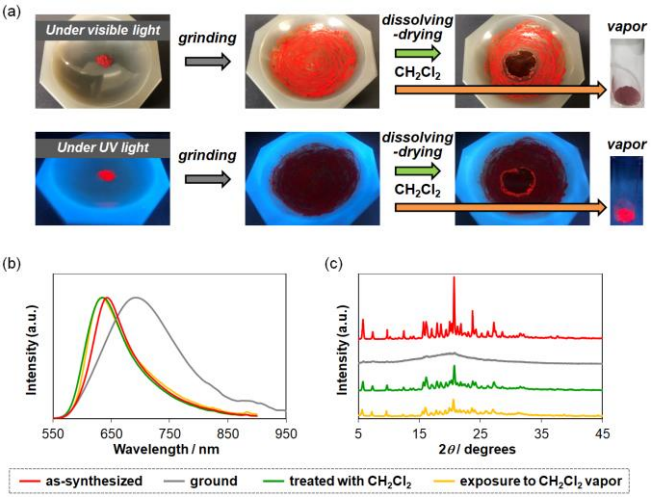

Figure 4. Mechanochromic luminescence behavior of **2-F**$^{2+}$(BF_4^-)$_2$. (a) Photographs of **2-F**$^{2+}$(BF_4^-)$_2$ under visible (top) and UV (bottom) light (λ_{ex} = 365 nm) in various states. (b) Emission spectra (λ_{ex} = 350 nm) and (c) PXRD patterns for as-synthesized **2-F**$^{2+}$(BF_4^-)$_2$ (red), ground **2-F**$^{2+}$(BF_4^-)$_2$ (gray), **2-F**$^{2+}$(BF_4^-)$_2$ recovered by treatment with CH_2Cl_2 after grinding (green), and **2-F**$^{2+}$(BF_4^-)$_2$ recovered by exposure to CH_2Cl_2 vapor after grinding (yellow).

On the other hand, upon grinding as-synthesized solids of **2-F**$^{2+}$(BF_4^-)$_2$, the luminescence color of macrocyclic dication clearly changed to deep red [λ_{em}/nm (Φ_{em}): 692 (0.01)]. This unique mechanochromic luminescence was accompanied by a crystal-to-amorphous transition confirmed by PXRD. The original emission color and crystallinity were recovered by treatment of

Table 1. Luminescence properties of **1-F**$^{+}$(BF_4^-), **2-F**$^{2+}$(BF_4^-)$_2$, **1-O**$^{+}$(BF_4^-), **2-O**$^{2+}$(BF_4^-)$_2$, and **2-O**$^{2+}$(PF_6^-)$_2$ in the solid state at 298K.
[a] Excitation at 350 nm. [b] Detection at the emission maximum.

	1-F^{+}(BF_4^-)						**2-F**$^{2+}$(BF_4^-)$_2$					
	λ_{em} / nm[a]	Φ_{em}[a]	τ_1 / ns	τ_2 / ns	τ_3 / ns	τ_{ave} / ns[b]	λ_{em} / nm[a]	Φ_{em}[a]	τ_1 / ns	τ_2 / ns	τ_3 / ns	τ_{ave} / ns[b]
as-synthesized crystals	609, 669	0.03	0.325	2.31	—	0.544	642	0.03	1.12	3.01	—	2.60
ground samples	604	0.01	0.071	0.304	2.10	0.198	692	0.01	0.416	1.61	5.05	2.80
dissolving (CH_2Cl_2)-drying process	599	0.02	0.240	0.797	—	0.327	634	0.03	1.07	4.28	—	3.52
exposure to CH_2Cl_2 vapor	600	0.02	0.209	1.23	—	0.295	634	0.02	0.738	1.65	—	1.27
	1-O^{+}(BF_4^-)						**2-O**$^{2+}$(PF_6^-)$_2$					
	λ_{em} / nm[a]	Φ_{em}[a]	τ_1 / ns	τ_2 / ns	τ_3 / ns	τ_{ave} / ns[b]	λ_{em} / nm[a]	Φ_{em}[a]	τ_1 / ns	τ_2 / ns	τ_3 / ns	τ_{ave} / ns[b]
as-synthesized crystals	624	0.05	3.22	—	—	3.22	599	0.02	0.441	—	—	0.441
ground samples	637	0.01	0.345	0.892	—	0.516	657	0.01	0.256	1.02	3.83	1.61
dissolving (CH_2Cl_2)-drying process	630	0.03	1.20	2.55	—	2.07	591	0.02	0.250	0.368	—	0.282
exposure to CH_2Cl_2 vapor	638	0.02	0.876	2.33	—	1.77	597	0.01	0.137	0.650	—	0.157

amorphous solids of **2-F**$^{2+}$(BF_4^-)$_2$ with CH_2Cl_2 followed by drying [λ_{em}/nm (Φ_{em}): 634 (0.03)] or by exposure to CH_2Cl_2 vapor [λ_{em}/nm (Φ_{em}): 634 (0.02)] (Figure 4 and Table 1).

Similar mechanochromic luminescence was observed for methoxyphenyl-substituted cations. As summarized in Table 1, as-synthesized powders of **1-O**$^{+}$(BF_4^-) and **2-O**$^{2+}$(BF_4^-)$_2$ exhibit red and orange emission [λ_{em}/nm (Φ_{em}): 624 (0.05) for **1-O**$^{+}$(BF_4^-) and 602 (0.03) for **2-O**$^{2+}$(BF_4^-)$_2$], respectively. Similar to fluorophenyl derivatives, monocation **1-O**$^{+}$(BF_4^-) exhibits longer-wavelength emission than **2-O**$^{2+}$(BF_4^-)$_2$, probably due to the difference in the packing structure. However, these cations do not show mechanochromic behavior. The solid-state emission of monocation **1-O**$^{+}$(BF_4^-) did not change, and the PXRD pattern of the ground solid is almost the same as that of the pristine crystal (Figure S9). For macrocyclic dication **2-O**$^{2+}$(BF_4^-)$_2$, the original emission of macrocyclic dication **2-O**$^{2+}$(BF_4^-)$_2$ did not recover because the amorphous state given by grinding is still present under treatment with CH_2Cl_2 followed by drying (Figure S10 and Table S4).

We next investigated the PF_6^- salt with the expectation of high crystallinity. As a result, reversible mechanochromic luminescence behavior was observed for **2-O**$^{2+}$(PF_6^-)$_2$ as in **2-F**$^{2+}$(BF_4^-)$_2$. Upon grinding the as-synthesized solids of **2-O**$^{2+}$(PF_6^-)$_2$, the luminescence color clearly changed from orange [λ_{em}/nm (Φ_{em}): 599 (0.02)] to deep red [λ_{em}/nm (Φ_{em}): 657 (0.01)], and then the original orange emission was recovered by treatment of amorphous solids of **2-O**$^{2+}$(PF_6^-)$_2$ with CH_2Cl_2 followed by drying [λ_{em}/nm (Φ_{em}): 591 (0.02)] or by exposure to CH_2Cl_2 vapor [λ_{em}/nm (Φ_{em}): 597 (0.01)] (Figure 5). Whereas a slight change in diffuse reflectance spectra was observed before and after grinding, the excitation spectrum of ground sample of **2-O**$^{2+}$(PF_6^-)$_2$ exhibit an obvious red-shift (Figure S11m,n). Thus, we concluded that the mechanochromic luminescence would be induced by a change in the intermolecular interaction in the excited state, i.e., the formation of excimer in the amorphous state.

We then examined the emission lifetimes, which were summarized in Tables 1 and S4 and Figure S11. Single exponential decay was observed in the emission decay curve of **2-O**$^{2+}$(PF_6^-)$_2$ (Figure S11o) and the lifetime was estimated to be 0.44 ns; thus, the orange emission was assigned to fluorescence. Upon grinding of as-synthesized powders, the emission decay curve of **2-O**$^{2+}$(PF_6^-)$_2$ showed triple exponential decay (Figure S11o) and the lifetimes were 0.26, 1.02, and 3.83 ns. This means that **2-O**$^{2+}$(PF_6^-)$_2$ in the amorphous state would contain multiple emissive species, such as excimer.

In this way, the mechanofluorochromic behavior was observed in tethered macrocyclic dications **2**$^{2+}$ with alkylene linkers in combination with a proper counterion, which can be easily modified by counterion exchange. Therefore, these macrocyclic dications **2**$^{2+}$ are quite rare examples of NIR-mechanochromic emission based on simple organic molecules, especially for carbocations.

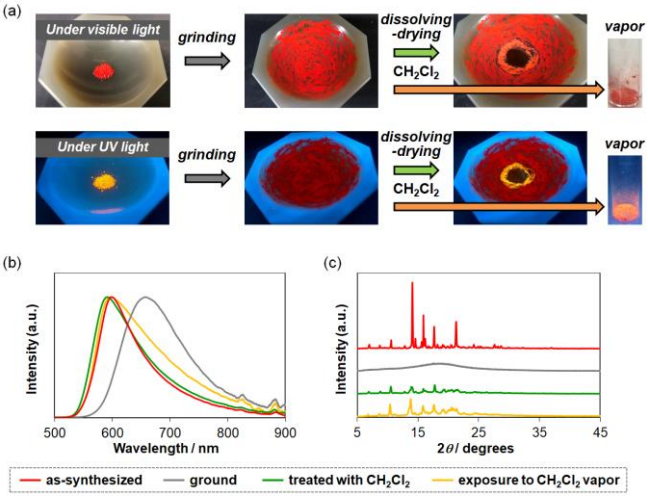

Figure 5. Mechanochromic luminescence behavior of **2-O**$^{2+}$(PF_6^-)$_2$. (a) Photographs of **2-O**$^{2+}$(PF_6^-)$_2$ under visible (top) and UV (bottom) light (λ_{ex} = 365 nm) in various states. (b) Emission spectra (λ_{ex} = 350 nm) and (c) PXRD patterns for as-synthesized **2-O**$^{2+}$(PF_6^-)$_2$ (red), ground **2-O**$^{2+}$(PF_6^-)$_2$ (gray), **2-O**$^{2+}$(PF_6^-)$_2$ recovered by treatment with CH_2Cl_2 after grinding (green), and **2-O**$^{2+}$(PF_6^-)$_2$ recovered by exposure to CH_2Cl_2 vapor after grinding (yellow).

Conclusion

In this study, we designed and synthesized novel macrocyclic dications **2-F**$^{2+}$ and **2-O**$^{2+}$ with alkylene spacers. During the synthesis, a key macrocyclic diketone **6**, which can be a versatile building block for constructing macrocyclic compounds, was prepared in good yield by using the "Thorpe-Ingold effect".[31] Whereas the reference monocations **1**$^{+}$ did not show

mechanochromic behavior due to their high crystallinity, tethered macrocyclic dications $\mathbf{2}^{2+}$ exhibited mechanochromic emission extending to the red region (-900 nm). PXRD and spectroscopic analyses revealed that such mechanochromic behavior was induced by the crystal-to-amorphous transition. The constrained structure of macrocyclic dications $\mathbf{2}^{2+}$ compared to that of monocations $\mathbf{1}^{+}$ is the key to realizing the change in the emission pattern, and the intermolecular interaction in the solid state can be changed by applying mechanical stimuli. To the best of our knowledge, this is the first example of mechanochromic luminescence based on carbocations. The design strategy in this study may open the door to creating a variety of stimuli-responsive materials such as NIR-mechanofluorochromic molecules.

Experimental Section

All reactions were carried out under an argon atmosphere. All commercially available compounds were used without further purification unless otherwise indicated. Column chromatography was performed on silica gel 60N (KANTO KAGAKU, spherical neutral) of particle size 40-50 μm or Wakogel® 60N (neutral) of particle size 38-100 μm. ^{1}H and ^{13}C NMR spectra were recorded on a BRUKER Ascend™ 400 (^{1}H/400 MHz and ^{13}C/100 MHz) spectrometer. IR spectra were measured on a Shimadzu IRAffinity-1S spectrophotometer using the attenuated total reflection (ATR) mode or as a KBr pellet on a JEOL JIR-WINSPEC100 FT/IR spectrophotometer. Mass spectra were recorded on a JEOL JMS-T100GCV spectrometer in FD mode (GC-MS & NMR Laboratory, Research Faculty of Agriculture, Hokkaido University). Melting points were measured on a Yamato MP-21 and are uncorrected. Elemental analyses were performed on an Exeter Analytical CE440 at the Center for Instrumental Analysis of Hokkaido University. UV/Vis spectra were recorded on a Hitachi U-3500 spectrophotometer. Emission spectra were recorded on a JASCO FP-8600 spectrofluorometer. Emission quantum yields were measured on a Hamamatsu Photonics C9920-02 system. Emission lifetimes were measured on a Hamamatsu Photonics Quantaurus-Tau C11367 system. Diffuse reflectance spectra were obtained using a Shimadzu UV-2400PC spectrophotometer equipped with integrating sphere apparatus. The reflectance spectra were converted to absorption spectra using the Kubelka–Munk function. Powder X-ray diffraction (PXRD) was conducted using a Bruker D8 Advance diffractometer equipped with a graphite monochromator using Cu-Kα radiation and a one-dimensional LinxEye detector. DFT calculations were performed with the Gaussian 16W program package.[37] The geometries of the compounds were optimized by using the B3LYP method in combination with the 6-31G* basis set unless otherwise indicated. Single-crystal X-ray structure analyses were performed by a Rigaku XtaLAB Synergy (Cu-Kα radiation, λ = 1.54184 Å) with HyPix diffractometer. Using Olex2,[38] the structure was solved with the SHELXT[39] structure solution program using Intrinsic Phasing and refined with the SHELXL[40] refinement package using Least Squares minimization. All the hydrogen atoms were located at the calculated positions and refined with riding.

Preparation of 5

4,4'-Dihydroxybenzophenone **3** (3.31 g, 15.4 mmol), **4**[30] (50.8 g, 123 mmol) and K_2CO_3 (17.1 g, 124 mmol) were suspended in DMF (200 mL) at 25 °C. The mixture was stirred at 120 °C for 14 h. After cooling to 25 °C, the resulting mixture was concentrated in *vacuo* to remove DMF, and the resulting residue was diluted with water and extracted with $CHCl_3$. The combined organic layers were washed with water and brine, and dried over anhydrous $MgSO_4$. After filtration, the solvent was concentrated under reduced pressure. The crude product was purified by column chromatography on silica gel ($CHCl_3$ only) and recrystallized from EtOH to give **5** (9.15 g) as a white solid in 85% yield.

Mp: 155-157 °C; ^{1}H NMR (400 MHz, $CDCl_3$): δ/ppm 7.75 (4H, d, *J* = 8.8 Hz), 7.72 (4H, d, *J* = 8.0 Hz), 7.22 (4H, d, *J* = 8.0 Hz), 6.80 (4H, d, *J* = 8.8 Hz), 3.93 (4H, s), 3.71 (4H, s), 2.38 (6H, s), 1.05 (12H, s); ^{13}C NMR (100 MHz, $CDCl_3$): δ/ppm 194.24, 161.92, 144.73, 132.76, 132.04, 130.86, 129.78, 127.83, 113.91, 74.43, 72.12, 35.58, 21.62, 21.53; IR (KBr): *ν*/cm^{-1} 3068, 3041, 2972, 2938, 2884, 2739, 2567, 1924, 1633, 1600, 1572, 1510, 1476, 1419, 1402, 1359, 1303, 1286, 1256, 1188, 1172, 1098, 1036, 1003, 963, 850, 836, 813, 781, 769, 670, 573, 557; LR-MS (FD) *m/z* (%): 697.17 (6), 696.17 (20), 695.18 (45), 694.17 (M^+, bp); Anal. Calcd. (%) for $C_{37}H_{42}O_9S_2 \cdot 0.5(H_2O)$: C 63.14, H 6.16; Found: C 63.31, H 6.03.

Preparation of 6

4,4'-Dihydroxybenzophenone **3** (467 mg, 2.18 mmol), **5** (1.50 g, 2.16 mmol) and Cs_2CO_3 (7.14 g, 21.9 mmol) were suspended in DMF (440 mL) at 25 °C. The mixture was stirred at 120 °C for 6 h. After cooling to 25 °C, the resulting mixture was extracted with $CHCl_3$ three times. The combined organic layers were washed with 1 M HCl aq. and brine, and dried over anhydrous $MgSO_4$. After filtration, the solvent was concentrated under reduced pressure. The crude product was purified by column chromatography on silica gel ($CHCl_3$/EtOAc = 30/1) and recrystallized from $CHCl_3$ / hexane to give **6** (401 mg) as a white solid in 33% yield.

Mp: 298-299 °C; ^{1}H NMR (400 MHz, $CDCl_3$): δ/ppm 7.45 (8H, d, *J* = 8.8 Hz), 6.77 (8H, d, *J* = 8.8 Hz), 3.90 (8H, s), 1.16 (12H, s); ^{13}C NMR (100 MHz, $CDCl_3$): δ/ppm 193.65, 162.17, 131.87, 130.44, 114.35, 72.27, 37.31, 22.01; IR (KBr): *ν*/cm^{-1} 3060, 2964, 2931, 2876, 1638, 1600, 1510, 1473, 1417, 1399, 1365, 1317, 1306, 1283, 1261, 1200, 1164, 1146, 1118, 1034, 1014, 985, 949, 929, 849, 841, 835, 767, 729, 688, 637, 628, 609, 567, 538, 497, 488, 464; LR-MS (FD) *m/z* (%): 566.23 (10), 565.23 (41), 564.23 (M^+, bp); Anal. Calcd. (%) for $C_{36}H_{36}O_6 \cdot 0.25(H_2O)$: C 75.97, H 6.46; Found: C 76.04, H 6.36. X-ray structure: CCDC 2223167.

Preparation of 7'-F via 7-F

To a solution of 4-bromofluorobenzene (780 μL, 7.15 mmol) in dry THF (20 mL) was added *n*BuLi (1.57 M solution in hexane, 4.50 mL, 7.07 mmol) dropwise over 8 min at –78 °C under Ar, and the mixture was stirred for 1 h. To the solution was added **6** (401 mg, 711 μmol) in dry THF (140 mL) at –78 °C. The mixture was gradually warmed up to 25 °C and stirred for 2 h. After being diluted with water, the whole mixture was extracted with EtOAc three times. The combined organic layers were washed with water and brine, and dried over anhydrous Na_2SO_4. After filtration, the solvent was concentrated under reduced pressure.

The crude product was washed with a mixture of CH_2Cl_2 and MeOH (1 : 1) to give **7'-F** (452 mg) as a white solid in 81% yield.

Mp: 147-148 °C; ^{1}H NMR (400 MHz, $CDCl_3$): δ/ppm 7.33 (2H, d, *J* = 8.8 Hz), 7.32 (2H, d, *J* = 8.8 Hz), 7.19 (8H, d, *J* = 8.8 Hz), 6.99 (2H, d, *J* = 8.8 Hz), 6.97 (2H, d, *J* = 8.8 Hz), 6.68 (8H, d, *J* = 8.8 Hz), 3.77 (4H, d, *J* = 8.8 Hz), 3.65 (4H, d, *J* = 8.8 Hz), 2.97 (6H, s), 1.10 (12H, s); ^{13}C NMR (100 MHz, $CDCl_3$): δ/ppm 161.98 (C, d, $J_{C\text{-}F}$ = 246 Hz), 157.59, 138.46 (C, d, $J_{C\text{-}F}$ = 3.2 Hz), 137.11, 132.03 (C, d, $J_{C\text{-}F}$ = 7.8 Hz), 128.39, 114.34 (C, d, $J_{C\text{-}F}$ = 21 Hz), 114.03, 86.08, 71.49, 51.72, 35.90, 22.14; IR (KBr): *ν*/cm^{-1} 3037, 2960, 2904, 2871, 2825, 1735, 1607, 1505, 1474, 1402, 1368, 1300, 1251, 1228, 1180, 1170, 1159, 1077, 1047, 1034, 996, 966, 914, 829, 729, 640, 621, 591, 566; LR-MS (FD) *m/z* (%): 786.36 (17), 785.36 (57), 784.36 (M^+, bp); HR-MS (FD) Calcd. For $C_{50}H_{50}F_2O_6$: 784.35755; Found: 784.35878. X-ray structure: CCDC 2223168.

Preparation of 7'-O via 7-O

To a solution of 4-bromoanisole (1.35 mL, 10.8 mmol) in dry THF (30 mL) was added *n*BuLi (1.64 M solution in hexane, 6.50 mL, 10.7 mmol) dropwise over 10 min at –78 °C under Ar, and the mixture was stirred for 1 h. To the solution was added **6** (597 mg, 1.06 mmol) in dry THF (210 mL) at –78 °C. The mixture was gradually warmed up to 24 °C and stirred for 2 h. After being diluted with water, the whole mixture was extracted with CH_2Cl_2 three times. The combined organic layers were washed with water and brine, and dried over anhydrous Na_2SO_4. After filtration, the solvent was concentrated under reduced pressure. The crude product was purified by reprecipitation from $CHCl_3$ and MeOH to give **7'-O** (785 mg) as a light-yellow solid in 92% yield.

Mp: 254-256 °C (decomp.); ^{1}H NMR (400 MHz, $CDCl_3$): δ/ppm 7.30-7.27 (4H, m), 7.23 (8H, d, *J* = 8.8 Hz), 6.83 (4H, dd, *J* = 2.0, 8.8 Hz), 6.67 (8H, d, *J* = 8.8 Hz), 3.81 (3H, s), 3.81 (3H, s), 3.77-3.60 (8H, m), 2.97 (6H, s), 1.10 (12H, t, *J* = 4.8 Hz); ^{13}C NMR (100 MHz, $CDCl_3$): δ/ppm 158.80, 157.36, 137.77, 134.30, 131.96, 128.22, 113.84, 112.79, 86.26, 71.22, 55.23, 51.62, 35.75, 22.17; IR (KBr): *ν*/cm^{-1} 3038, 2957, 2871, 2833, 1608, 1582, 1507, 1475, 1400, 1365, 1301, 1252, 1175, 1116, 1076, 1037, 965, 915, 827, 731, 621, 595; LR-MS (FD) *m/z* (%): 823.41 (7), 822.41 (11), 810.40 (20), 809.39 (61), 808.39 (M^+, bp), 778.38 (11), 777.36 (8); Anal. Calcd. (%) for $C_{52}H_{56}O_8 \cdot 0.25(H_2O)$: C 76.77, H 7.00; Found: C 76.85, H 6.99.

Preparation of 2-F^{2+}(BF_4^-)$_2$

To a mixture of dry CH_2Cl_2 (20 mL) and propionic anhydride (3 mL) was added 42% HBF_4 aq. (80 µL, 532 µmol) at 0 °C under Ar, and the mixture was stirred for 1 h at 26 °C. To the solution was added **7'-F** (101 mg, 129 µmol) at 0 °C, and the mixture was stirred for 1 h at 0 °C. The addition of dry diethyl ether led to precipitation of the dication salt. The precipitates were collected, washed with dry diethyl ether three times, and dried *in vacuo* to give **2-F**$^{2+}$(BF_4^-)$_2$ (83.1 mg) as a red-brown powder in 72% yield.

Mp: 199-204 °C (decomp.); ^{1}H NMR (400 MHz, CD_3CN): δ/ppm 7.38 (2H, d, *J* = 8.8 Hz), 7.36 (2H, d, *J* = 8.8 Hz), 7.32 (8H, d, *J* = 8.8 Hz), 7.26 (2H, d, *J* = 8.8 Hz), 7.25 (2H, d, *J* = 8.8 Hz), 7.17 (8H, d, *J* = 8.8 Hz), 4.27 (8H, s), 1.29 (12H, s); ^{13}C NMR (100 MHz, CD_3CN): δ/ppm 192.61, 172.00, 169.42 (C, d, $J_{C\text{-}F}$ = 262 Hz), 144.84, 141.51 (C, d, $J_{C\text{-}F}$ = 11 Hz), 135.71 (C, d, $J_{C\text{-}F}$ = 2.0 Hz), 132.17, 118.14, 117.48 (C, d, $J_{C\text{-}F}$ = 22 Hz), 74.22, 37.95, 21.12; IR (KBr): *ν*/cm^{-1} 3102, 2966, 2877, 2733, 2607, 1585, 1506, 1475, 1440, 1416, 1368, 1317, 1280, 1246, 1198, 1168, 1127, 1059, 984, 916, 853, 766, 728, 670, 647, 621, 590, 571, 521, 507, 424, 410; LR-MS (FD) *m/z* (%): 810.31 (16), 809.30 (30), 808.29 (7), 762.30 (23), 761.30 (64), 760.30 ([M^{2+}+F^-]$^+$, bp), 759.30 (47), 758.30 (78), 757.31 (33), 756.30 (54), 743.30 (13), 742.30 (36), 741.31 (54), 740.31 (36), 739.30 (58), 738.29 (17), 361.15 (M^{2+}, 5); HR-MS (FD) Calcd. For $C_{48}H_{44}F_2O_4$: 722.31967; Found: 722.32169; UV/Vis (CH_2Cl_2): λ_{max} / nm (*ε* / 10^4 M^{-1} cm^{-1}) 480 (12.4), 420 (6.01), 267 (2.08). X-ray structure: CCDC 2223170.

Preparation of 2-O^{2+}(BF_4^-)$_2$

To a mixture of dry CH_2Cl_2 (20 mL) and propionic anhydride (3 mL) was added 42% HBF_4 aq. (80 µL, 532 µmol) at 0 °C under Ar, and the mixture was stirred for 1 h at 26 °C. To the solution was added **7'-O** (103 mg, 127 µmol) at 0 °C, and the mixture was stirred for 1 h at 0 °C. The addition of dry diethyl ether led to precipitation of the dication salt. The precipitates were collected, washed with dry diethyl ether three times, and dried *in vacuo* to give **2-O**$^{2+}$(BF_4^-)$_2$ (113 mg) as a red powder in 97% yield.

Mp: 165-170 °C (decomp.); ^{1}H NMR (400 MHz, CD_3CN): δ/ppm 7.27 (4H, d, *J* = 8.8 Hz), 7.23 (8H, d, *J* = 8.8 Hz), 7.14 (6H, d, *J* = 8.8 Hz), 7.12 (6H, d, *J* = 8.8 Hz), 4.21 (8H, s), 4.05 (6H, s), 1.27 (12H, s); ^{13}C NMR (100 MHz, CD_3CN): δ/ppm 191.54, 170.72, 170.24, 143.51, 143.16, 132.22, 131.77, 117.44, 116.59, 73.75, 57.49, 37.94, 21.20; IR (KBr): *ν*/cm^{-1} 2963, 1583, 1507, 1440, 1366, 1315, 1275, 1167, 1125, 1083, 1061, 917, 852, 766, 593, 419; LR-MS (FD) *m/z* (%): 835.30 (10), 834.30 (30), 833.30 ([M^{2+}+BF_4^-]$^+$, 57), 832.30 (13), 784.30 (6), 783.31 (5), 782.31 (11), 781.31 (12), 780.31 (19), 767.31 (6), 766.31 (17), 765.31 (33), 764.31 (36), 763.31 (61), 748.31 (6), 747.31 ([M+H]$^+$, 10), 374.15 (20), 373.65 (61), 373.15 (M^{2+}, bp); Anal. Calcd. (%) for $C_{50}H_{50}B_2F_8O_6 \cdot 0.5(CH_2Cl_2)$: C 62.99, H 5.34; Found: C 62.70, H 5.38; UV/Vis (CH_2Cl_2): λ_{max} / nm (*ε* / 10^4 M^{-1} cm^{-1}) 476 (13.8), 271 (4.25).

Preparation of 2-O^{2+}(PF_6^-)$_2$

To a mixture of dry CH_2Cl_2 (90 mL) and propionic anhydride (13.5 mL) was added 60% HPF_6 aq. (310 µL, 2.26 mmol) at 0 °C under Ar, and the mixture was stirred for 1 h at 0 °C. To the solution was added **7'-O** (454 mg, 561 µmol) at 0 °C, and the mixture was stirred for 1 h at 0 °C. The addition of dry diethyl ether led to precipitation of the dication salt. The precipitates were collected, washed with dry diethyl ether three times, and dried *in vacuo* to give **2-O**$^{2+}$(PF_6^-)$_2$ (503 mg) as a red powder in 87% yield.

Mp: 138-143 °C (decomp.); ^{1}H NMR (400 MHz, CD_3CN): δ/ppm 7.24 (4H, d, *J* = 8.8 Hz), 7.21 (8H, d, *J* = 8.8 Hz), 7.12 (6H, d, *J* = 8.8 Hz), 7.09 (6H, d, *J* = 8.8 Hz), 4.18 (8H, s), 4.02 (6H, s), 1.25 (12H, s); ^{13}C NMR (100 MHz, CD_3CN): δ/ppm 191.60, 170.74, 170.23, 143.51, 143.18, 132.22, 131.78, 117.43, 116.60, 73.74, 57.48, 37.94, 21.20; IR (ATR): *ν*/cm^{-1} 2968, 2939, 2603, 1815, 1730, 1577, 1507, 1477, 1465, 1438, 1361, 1315, 1299, 1272, 1259, 1154, 1125, 997, 921, 829, 767, 731, 671, 650, 623, 591, 576, 556, 529, 512, 420; LR-MS (FD) *m/z* (%): 893.32 (18), 892.32 (60), 891.32 ([M^{2+}+PF_6^-]$^+$, bp), 781.36 (7), 780.35 (12), 764.35 (8), 763.35 (14), 374.18 (6), 373.68 (21), 373.18 (M^{2+}, 37); HR-MS (FD) Calcd. For $C_{50}H_{50}O_6$: 746.36074; Found: 746.36233. X-ray structure: CCDC 2223171.

Acknowledgements

The authors thank Prof. Dr. Masako Kato and Dr. Masaki Yoshida (Kwansei Gakuin University) for the measurements of solid-state samples. This work was supported by Grant-in-Aid from MEXT and JSPS (Nos. JP20H02719 and JP20K21184 to T.S., and JP21H01912 and JP21H05468 to Y.I.). Y.I. acknowledges the 2020 DIC Award in Synthetic Organic Chemistry, Japan, and the Foundation of the Promotion of Ion Engineering.

Keywords: carbocations • macrocycles • solid-state emission • red emission • mechanochromism

[1] R. R. Naredla, D. A. Klumpp, *Chem. Rev.* **2013**, *113*, 6905–6948.
[2] D. F. Duxbury, *Chem. Rev.* **1993**, *93*, 381–433.
[3] J. Bosson, J. Gouin, J. Lacour, *Chem. Soc. Rev.* **2014**, *43*, 2824–2840.
[4] T. J. Sørensen, C. B. Hildebrandt, J. Elm, J. W. Andreasen, A. Ø. Madsen, F. Westerlund, B. W. Laursen, *J. Mater. Chem.* **2012**, *22*, 4797–4805.
[5] H. Noguchi, T. Hirose, S. Yokoyama, K. Matsuda, *CrystEngComm* **2016**, *18*, 7377–7383.
[6] M. Rosenberg, K. R. Rostgaard, Z. Liao, A. Ø. Madsen, K. L. Martinez, T. Vosch, B. W. Laursen, *Chem. Sci.* **2018**, *9*, 3122–3130.
[7] A. Samanta, K. R. Gopidas, P. K. Das, *J. Phys. Chem.* **1993**, *97*, 1583–1588.
[8] Y. Zheng, X. Zheng, Y. Xiang, A. Tong, *Chem. Commun.* **2017**, *53*, 11130–11133.
[9] J. Mei, N. L. C. Leung, R. T. K. Kwok, J. W. Y. Lam, B. Z. Tang, *Chem. Rev.* **2015**, *115*, 11718–11940.
[10] M. Shimizu, T. Hiyama, *Chem. Asian J.* **2010**, *5*, 1516–1531.
[11] F. Würthner, *Angew. Chem. Int. Ed.* **2020**, *59*, 14192–14196.
[12] Z. Chi, X. Zhang, B. Xu, X. Zhou, C. Ma, Y. Zhang, S. Liu, J. Xu, *Chem. Soc. Rev.* **2012**, *41*, 3878–3896.
[13] Y. Q. Dong, J. W. Y. Lam, B. Z. Tang, *J. Phys. Chem. Lett.* **2015**, *6*, 3429–3436.
[14] S. Ito, *Chem. Lett.* **2021**, *50*, 649–660.
[15] X. Cheng, D. Li, Z. Zhang, H. Zhang, Y. Wang, *Org. Lett.* **2014**, *16*, 880–883.
[16] M. Tanioka, S. Kamino, A. Muranaka, Y. Ooyama, H. Ota, Y. Shirasaki, J. Horigome, M. Ueda, M. Uchiyama, D. Sawada, S. Enomoto, *J. Am. Chem. Soc.* **2015**, *137*, 6436–6439.
[17] M. Okazaki, Y. Takeda, P. Data, P. Pander, H. Higginbotham, A. P. Monkman, S. Minakata, *Chem. Sci.* **2017**, *8*, 2677–2686.
[18] J. Chen, D. Li, W. Chi, G. Liu, S. H. Liu, X. Liu, C. Zhang, J. Yin, *Chem. Eur. J.* **2018**, *24*, 3671–3676.
[19] C. Wang, Z. Li, *Mater. Chem. Front.* **2017**, *1*, 2174–2194.
[20] T. Suzuki, T. Fukushima, T. Miyashi, T. Tsuji, *Angew. Chem. Int. Ed. Engl.* **1997**, *36*, 2495–2497.
[21] Y. Sagara, T. Mutai, I. Yoshikawa, K. Araki, *J. Am. Chem. Soc.* **2007**, *129*, 1520–1521.
[22] H. Ito, T. Saito, N. Oshima, N. Kitamura, S. Ishizaka, Y. Hinatsu, M. Wakeshima, M. Kato, K. Tsuge, M. Sawamura, *J. Am. Chem. Soc.* **2008**, *130*, 10044–10045.
[23] H. Ito, M. Muromoto, S. Kurenuma, S. Ishizaka, N. Kitamura, H. Sato, T. Seki, *Nat. Commun.* **2013**, *4*, 2009.
[24] Y. Sagara, S. Yamane, M. Mitani, C. Weder, T. Kato, *Adv. Mater.* **2016**, *28*, 1073–1095.
[25] Y. Ishigaki, K. Sugawara, M. Yoshida, M. Kato, T. Suzuki, *Bull. Chem. Soc. Jpn.* **2019**, *92*, 1211–1217.
[26] Y. Matsuo, Y. Wang, H. Ueno, T. Nakagawa, H. Okada, *Angew. Chem. Int. Ed.* **2019**, *58*, 8762–8767.
[27] T. Nishiuchi, H. Sotome, R. Fukuuchi, K. Kamada, H. Miyasaka, T. Kubo, *Aggregate* **2021**, *2*, e126.
[28] T. Mori, K. Sekine, K. Kawashima, T. Mori, Y. Kuninobu, *Eur. J. Org. Chem.* **2022**, e202200873.
[29] R. D. Crocker, D. P. Pace, B. Zhang, D. J. M. Lyons, M. M. Bhadbhade, W. W. H. Wong, B. K. Mai, T. V. Nguyen, *J. Am. Chem. Soc.* **2021**, *143*, 20384–20394.
[30] N. Rozentul, Y. Avrahami, M. Shubely, L. Levy, A. Munder, G. Cohen, E. Cerasi, S. Sasson, A. Gruzman, *Pharm. Res.* **2017**, *34*, 2873–2890.
[31] M. E. Jung, G. Piizzi, *Chem. Rev.* **2005**, *105*, 1735–1766.
[32] A. Bondi, *J. Phys. Chem.* **1964**, *68*, 441–451.
[33] M. Horn, H. Mayr, *Chem. Eur. J.* **2010**, *16*, 7469–7477.
[34] G. Dyker, M. Hagel, O. Muth, C. Schirrmacher, *Eur. J. Org. Chem.* **2006**, 2134–2144.
[35] M. Kasha, *Radiat. Res.* **1963**, *20*, 55–70.
[36] N. J. Hestand, F. C. Spano, *Chem. Rev.* **2018**, *118*, 7069–7163.
[37] M. J. Frisch, G. W. Trucks, H. B. Schlegel, G. E. Scuseria, M. A. Robb, J. R. Cheeseman, G. Scalmani, V. Barone, G. A. Petersson, X. Nakatsuji, H.; Li, M. Caricato, A. V. Marenich, J. Bloino, B. G. Janesko, R. Gomperts, B. Mennucci, H. P. Hratchian, J. V. Ortiz, A. F. Izmaylov, J. L. Sonnenberg, D. Williams-Young, F. Ding, F. Lipparini, F. Egidi, J. Goings, B. Peng, A. Petrone, T. Henderson, D. Ranasinghe, V. G. Zakrzewski, J. Gao, N. Rega, G. Zheng, W. Liang, M. Hada, M. Ehara, K. Toyota, R. Fukuda, J. Hasegawa, M. Ishida, T. Nakajima, Y. Honda, O. Kitao, H. Nakai, T. Vreven, K. Throssell, J. A. J. Montgomery, J. E. Peralta, F. Ogliaro, M. J. Bearpark, J. J. Heyd, E. N. Brothers, K. N. Kudin, V. N. Staroverov, T. A. Keith, R. Kobayashi, J. Normand, K. Raghavachari, A. P. Rendell, J. C. Burant, S. S. Iyengar, J. Tomasi, M. Cossi, J. M. Millam, M. Klene, C. Adamo, R. Cammi, J. W. Ochterski, R. L. Martin, K. Morokuma, O. Farkas, J. B. Foresman, D. J. Fox, *Gaussian 16, Revision B.01*, Gaussian, Inc., Wallingford CT, 2016, **n.d.**
[38] O. V. Dolomanov, L. J. Bourhis, R. J. Gildea, J. A. K. Howard, H. Puschmann, *J. Appl. Crystallogr.* **2009**, *42*, 339–341.
[39] G. M. Sheldrick, *Acta Crystallogr. Sect. A Found. Adv.* **2015**, *71*, 3–8.
[40] G. M. Sheldrick, *Acta Crystallogr. Sect. C Struct. Chem.* **2015**, *71*, 3–8.

Entry for the Table of Contents

Insert graphic for Table of Contents here.

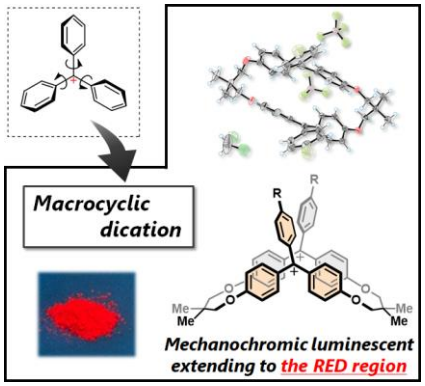

Since triarylmethyliums absorb visible light, their emissions can be extended to longer wavelengths than their absorptions. The constrained structure of macrocyclic dications is the key to realizing the emission extending to the red region. Thus, tethered macrocyclic dications exhibit NIR-mechanofluorochromism induced by the crystal-to-amorphous transition.

Institute and/or researcher Twitter usernames: Yusuke Ishigaki (@ysk_isgk); Laboratory (@Yuuichi_Hokudai)